Available online at www.sciencedirect.com
SCIENCE DIRECT
Cement and Concrete Research 36 (2006) 39–53
Cement and Concrete Research

# Polymorphism of tricalcium silicate, the major compound of Portland cement clinker
## 1. Structural data: review and unified analysis

F. Dunstetter[a,*], M.-N. de Noirfontaine[a,b], M. Courtial[c]

[a]Laboratoire des Solides Irradiés, Ecole Polytechnique, 91128 Palaiseau Cedex, France
[b]CECM-CNRS, 15 rue Georges Urbain, 94407 Vitry-sur-Seine, France
[c]Laboratoire d'Artois Mécanique et Habitat, Université d'Artois, route de l'Université, 62408 Béthune, France

Received 1 April 2004; accepted 1 December 2004

**Abstract**

This paper reviews the literature devoted to structural investigations, with a special concern to the various notations used by different authors. A unified analysis of the known T1, M1, M3 and R polymorphs is proposed. The superstructure relations between the various unit cells are discussed, together with the evidence of common 1D and 2D structural elements in all these polymorphs. These structural elements are related to the observed properties.


*Keywords:* Alite, $Ca_3SiO_5$; Clinker; Crystal structure, Polymorphism

## 1. Introduction

This paper reviews the literature and presents a unified analysis of the crystal structure of the known polymorphs of tricalcium silicate. A forthcoming paper will use the various models discussed here to perform Rietveld analyses of X-ray powder diffraction data of industrial clinkers.

Anhydrous Portland cement is essentially made of a synthetic rock, referred to as "clinker", which contains at least four major phases. Alite and belite are two solid solutions of two calcium silicates, $Ca_3SiO_5$ and $Ca_2SiO_4$, respectively, with a few percent of impurities. Two calcium aluminate phases are also observed: they constitute an interstitial phase between the larger crystals of both silicates. Within the compact mineralogical stoechiometric notation, C=CaO, S=$SiO_2$, A=$Al_2O_3$, F=$Fe_2O_3$ these compounds are designated as $C_3S$, $C_2S$, $C_3A$ and $C_4AF$. Either $C_3S$ or tricalcium silicate will be used as generic names for the phases with or without impurities. Whenever the presence of impurities is important for the discussion, a distinction between alite and "pure" tricalcium silicate will be made.

The structures of dicalcium silicate ($C_2S$) and the aluminates $C_3A$ and $C_4AF$ are relatively well known since structural models are available from the literature for all their polymorphs ($C_2S$: [1,2]; $C_3A$: [3,4]; $C_4AF$: [5,6]). This is not the case for the major phase, tricalcium silicate $C_3S$, which exhibits a complex polymorphism still not fully understood.

This paper is organised as follows. The first part is devoted to a chronological review of the structural studies of tricalcium silicate, including a clarification of the different notations used in the literature to name a given polymorph. The aim of the second part is to highlight the superstructure links between the various structures and to propose a revisited description of the average structure of the polymorphs. 1D and 2D structural objects are introduced and discussed in relation with the effects of some impurities on the structure and with the orientational disorder of silicates.

* Corresponding author. Tel.: +33 1 5670 3054; fax: +33 1 4675 0433.
*E-mail address:* dunstetter@cecm.cnrs.fr (F. Dunstetter).

0008-8846/$ - see front matter © 2004 Elsevier Ltd. All rights reserved.
doi:10.1016/j.cemconres.2004.12.003

## 2. Polymorphism of $C_3S$: chronological review of the literature

### 2.1. The polymorphs and their various notations

Tricalcium silicate exhibits seven polymorphs depending on temperature or impurities. In his famous text book, Taylor used the following notations [7]: T1, T2, T3 for the three triclinic forms, M1, M2, M3 for the three monoclinic forms, and R for the rhombohedral one. Both Roman and Arabic figures can be found in the literature: in the present paper, we have chosen the Arabic figures.

Due to very similar X-ray diffraction patterns and very low transformation enthalpies, these polymorphs have been difficult to distinguish. They were identified by combining differential thermal analysis (DTA), X-ray diffraction (XRD) [8–13] and optical microscopy [14] (see Table 1). In pure $C_3S$, the M3 polymorph was observed only by high temperature light microscopy. To observe it by other techniques, it was necessary to dope it with impurities. For the monoclinic polymorphs, there has been some confusion in defining and naming these polymorphs: for example, reported monoclinic MIb [15] and MIIb [13] forms are identical with the M3 polymorph [16]. Equivalent notations of the polymorphs used by different authors can be found in Table 2.

Pure tricalcium silicate exhibits seven polymorphs between room temperature and 1070 °C, according to the following sequence:

$$T1 \xleftrightarrow{620\ ^{o}C} T2 \xleftrightarrow{920\ ^{o}C} T3 \xleftrightarrow{980\ ^{o}C} M1 \xleftrightarrow{990\ ^{o}C} M2 \xleftrightarrow{1060\ ^{o}C} M3 \xleftrightarrow{1070\ ^{o}C} R$$

Depending on the impurities, various polymorphs can be stabilised at room temperature [11–13,15,17,18]. The M1 and M3 polymorphs are the most frequently observed in industrial clinkers [19–21]. Maki and co-workers have shown that the M1 and M3 polymorphs can be distinguished by means of birefringence measurements.

### 2.2. Crystallographic data of $C_3S$: unit cell parameters and structural models

The unit cell parameters of the various polymorphs are given in Table 3. They were determined either by single crystal or by powder diffraction experiments.

The first and pioneering work was that of Jeffery in early 1950s [8–10]. Using Weissenberg method, he was able to investigate various single crystals: pure $C_3S$ and alite, the latter either recrystallized from molten $CaCl_2$ (MgO and $Al_2O_3$ impurities) or extracted from clinkers (MgO, $Al_2O_3$, FeO, $Fe_2O_3$, MnO and $P_2O_5$ impurities). Pure $C_3S$ and alite were shown to be triclinic (T1 polymorph) and monoclinic (M3 polymorph), respectively. In his thesis work [8], Jeffery made the hypothesis of a true rhombohedral structure for the high temperature polymorph (R). He determined a pseudo-rhombohedral average structure (space group $R3m$; $a$=7.0 Å, $c$=25.0 Å) that he considered as a

Table 1
The seven polymorphs of tricalcium silicate observed by X-ray diffraction (XRD), differential thermal analysis (DTA) and optical microscopy: XRD and DTA results on pure $C_3S$ or alite [12,13], and optical microscopy observations on pure $C_3S$ [14]

| $T$ (°C) | XRD | DTA | | Microscopy |
|---|---|---|---|---|
| | | Observed signal | (cal $g^{-1}$) | |
| 1070 | R<br>pure | MIIb→R<br>None | – | R<br>M3→R: twinning and optical distinct properties |
| 1060 | MIIb<br>ZnO-doped | MIIa→MIIb<br>None | – | M3<br>(M1,M2)→M3: twinning and optical distinct properties |
| 990 | MIIa<br>pure | MIa→MIIa<br>Weak reversible signal | 0.05 | M1, M2<br>no difference |
| 980 | MIa<br>pure | TIII→MIa<br>Intense signal, brief; reversible, weak hysteresis (10 °C) | 0.5 | T3→M1: twinning and optical distinct properties |
| 920 | TIII<br>pure | TII→TIII<br>Intense signal, brief; reversible, without hysteresis | 1 | T2, T3<br>no difference |
| 620 | TII<br>pure | TI→TII<br>Large signal; reversible; strong hysteresis (20–40 °C) on cooling | 0.6 | T1→(T2, T3): distinct optical properties |
| 20 | TI<br>pure | None | – | T1 |

T=triclinic, M=monoclinic, R=rhombohedral.

Table 2
Different notations for the seven polymorphs of tricalcium silicate and their location in the literature

| T1 | T2 | T3 | M1 | M2 | M3 | R |
|---|---|---|---|---|---|---|
| Triclinic: Jeffery [8–10]; Il'inets [46] | | | Monoclinic, pseudo-orthorhombic: Yamaguchi [53] | | Monoclinic: Jeffery [8–10] | Rhombohedral: Jeffery [8–10]; Il'Inets [26]; Nishi [25] |
| TI: Bigaré [11]; Eysel [15]; Golovastikov [24]; Guinier [12]; Hahn [17]; Il'inets [47]; Regourd [13,48–50]; Sinclair [30]; Urabe [42,43]; Woermann [18] | TII: Bigaré [11]; Eysel [15]; Guinier [12]; Hahn [17]; Il'inets [47]; Regourd [13,48–50]; Sinclair [30]; Urabe [42,43]; Woermann [18] | TIII: Bigaré [11]; Eysel [15]; Guinier [12]; Hahn [17]; Il'inets [47]; Regourd [13,48–50]; Sinclair [30]; Urabe [42,43]; Woermann [18] | MI: Bigaré [11]; Guinier [12]; Hahn [17]; Regourd [48–50]; Sinclair [30]; Urabe [42,43]; Woermann [18] | MII: Bigaré [11]; Guinier [12]; Hahn [17]; Regourd [48–50]; Sinclair [30]; Urabe [42,43]; Woermann [18] | MIII: Guinier [12]; Il'inets [47]; Sinclair [30]; Urabe [42,43] | R=R($a$,$c$): Bigaré [11]; Eysel [15]; Guinier [12]; Hahn [17]; Maki [14,54]; Nishi [16]; Regourd [48–50,52]; Taylor [7]; Urabe [42,43]; Woermann [18] |
| | | | MIa: Eysel [15]; Regourd [13,51] | MIIa: Eysel [15]; Regourd [13,51] | MIIb: Regourd [13,51] MIb: Eysel [13] | R=R(2$a$,$c$): Il'inets [47] |
| T1: Maki [14,19]; Regourd [52]; Taylor [7] | T2: Maki [14,19]; Taylor [7] | T3: Maki [14,19]; Taylor [7] | M1: Maki [14,19–21,54]; Taylor [7] | M2: Maki [14,19,21]; Regourd [52]; Taylor [7] | M3: Maki [14,19–21,54]; Nishi [16]; Regourd [52]; Taylor [7] | |
| T: Nishi [16] | | | | | | |

According to Taylor [7], the notations T1, T2, T3, M1, M2, M3, R are now accepted. Each column is devoted to a given polymorph, including its different names. For example, M3 has been called MIII, MIIb or M1b.

valid approximation for all the true structures. The structure is based on calcium ions, silicate ions[1] and isolated oxide ions, each lying in a separate column parallel to the hexagonal $\mathbf{c}_H$ axis, each oxide ions being octahedrally coordinated by calcium. Two of the three independent silicate tetrahedra have the same orientation. Due to the very large unit cell, from the Weissenberg data, it was not possible to derive an atomic model for the M3 alite itself. But from the extra Bragg spots, Jeffery was able to determine the true symmetry of the lattice (space group $Cm$; $a$=33.08 Å, $b$=7.07 Å, $c$=18.56 Å, $\beta$=94.17°) and the metric relations between this large unit cell and his pseudo-rhombohedral average unit cell.

The first systematic work on powder samples was performed later by Regourd, Guinier and co-workers [11,12,22,23], including the six polymorphs of pure $C_3S$ between room temperature and melting point. The similar patterns observed for the different modifications clearly revealed the same underlying average structure, with displacive transformations between the polymorphs. Weak reflections in the powder diagrams suggested superstructures. The orthohexagonal pseudo-symmetry exhibited by tricalcium silicate was described by using either pseudo-hexagonal H or pseudo-orthorhombic OH (orthohexagonal) unit cells, with monoclinic or triclinic sets of cell parameters. By indexing all the monoclinic and triclinic polymorphs in the same[2] pseudo-orthorhombic or pseudo-hexagonal unit cells (Table 3), Regourd et al. [11–13] showed how each polymorph could be identified in two narrow angular ranges ($2\theta_{Cu}$=32–33° and $2\theta_{Cu}$=60–62°) by one characteristic splitting sequence of the rhombohedral reflections. The powder diffraction patterns allowed to determine the dimensions and symmetries of the various lattices, but gave no information on the structures. The monoclinic $Cm$ and triclinic $P1$[3] or $C1$ space groups were respectively proposed for the three monoclinic and triclinic polymorphs since they are subgroups of the $R3m$ space group of the high temperature polymorph. Another interesting result is that the monoclinic M3 polymorph found by Jeffery is never observed in the pure compound. It only appears in doped compounds (with ZnO or MgO impurities).

More than 20 years elapsed after Jeffery's first results before the resolution of the structure of another polymorph: the T1 structure was established by Golovastikov et al.

[1] The silicate ions are independent and not linked into chains or sheets.

[2] With a doubling of the $a$ and $b$ cell parameters in the triclinic polymorph, suggesting a possible superstructure.

[3] A triclinic pseudo-hexagonal (H) unit cell with $P1$ space group becomes a pseudo-orthohexagonal (OH) non-primitive unit cell with the $C1$ space group.

Table 3
Crystallographic data of the seven polymorphs known for tricalcium silicate

| Sample | | Reference | Space group | | $a$ (Å) | $b$ (Å) | $c$ (Å) | $\alpha$ (°) | $\beta$ (°) | $\gamma$ (°) | $V$ (Å$^3$) | $Z$ |
|---|---|---|---|---|---|---|---|---|---|---|---|---|
| R, pseudo-structure | S | Jeffery, 1952 [9] | $R3m$ | H | 7 | 7 | 25 | 90 | 90 | 120 | 1061 | 9 |
| | | | | OH | 12.124 | 7 | 25 | 90 | 90 | 90 | 2122 | |
| $C_3S$: $T$=1100 °C | P | Bigare et al., 1967 [11] | $R3m$ | H | 7.15 | 7.15 | 25.560 | 90 | 90 | 120 | 1132 | 9 |
| | P | Guinier and Regourd, 1969 [12] | | OH | 12.384 | 7.15 | 25.560 | 90 | 90 | 90 | 2263 | |
| $Ca_{2.98}Si_{0.98}Al_{0.04}O_5$: $T$=1200 °C | S | Nishi and Takéuchi, 1984 [25] | $R3m$ | H | 7.135 | 7.135 | 25.586 | 90 | 90 | 120 | 1128 | 9 |
| | | | | OH | 12.358 | 7.135 | 25.586 | 90 | 90 | 90 | 2256 | |
| $C_3S$, SrO-doped: $T$=1400 °C | | Il'inets and Malinovskii, 1985 [26] | $R3m$ | H | 7.0567 | 7.0567 | 24.974 | 90 | 90 | 120 | 1078 | 9 |
| | | | | OH | 12.222 | 7.0567 | 24.974 | 90 | 90 | 90 | 2256 | |
| M3, $C_3S$ + (MgO, $Al_2O_3$) | S | Jeffery, 1952 [9] | $Cm$ | | 33.08 | 7.07 | 18.56 | 90 | 94.17 | 90 | 4330 | 36 |
| | | | | OH | 12.245 | 7.07 | 25.004 | 90 | 90.01 | 90 | 2165 | |
| $C_3S$ + 0.5% ZnO: $T$=1020–90°C | P | Regourd, 1979 [13] | | OH | 12.372 | 7.123 | 25.440 | 90 | 90 | 90 | 2242 | ? |
| $Ca_{2.89}SiMg_{0.11}O_5$ | S | Nishi et al., 1985 [16] | $Cm$ | | 33.083 | 7.027 | 18.499 | 90 | 94.12 | 90 | 4289 | 36 |
| | | | | OH | 12.242 | 7.027 | 24.932 | 90 | 90.14 | 90 | 2145 | |
| Alite from a clinker | S | Mumme, 1995 [31] | $Cm$ | | 12.235 | 7.073 | 9.298 | 90 | 116.31 | 90 | 721 | 6 |
| | | | | OH | 12.235 | 7.073 | 25.005 | 90 | 89.71 | 90 | 2164 | 6 |
| | P | de Noirfontaine et al. [35,44] | | OH | 12.2313 | 7.033 | 24.9573 | 90 | 90.09 | 90 | 2147 | |
| M2, $C_3S$: $T$=1000 °C | P | Bigare et al., 1967 [11] | $Cm$ | OH | 12.342 | 7.143 | 25.434 | 90 | 90 | 90 | 2242 | ? |
| $C_3S$+0.5% ZnO: $T$=990°C | P | Regourd, 1979 [13] | ? | OH | 12.333 | 7.137 | 25.442 | 90 | 90 | 90 | 2239 | ? |
| M1, $C_3S$: $T$=980 °C | P | Bigare et al., 1967 [11] | $Cm$ | OH | 12.332 | 7.142 | 25.420 | 90 | 89.95 | 90 | 2239 | ? |
| | | Taylor, 1964 [55] | ? | OH | 12.426 | 7.045 | 24.985 | 90 | 90.07 | 90 | 2155 | ? |
| | P | de Noirfontaine et al. [35,44] | | OH | 12.2575 | 7.059 | 25.0462 | 90 | 90.06 | 90 | 2167 | |
| T3, $C_3S$: $T$=940 °C | P | Bigare et al., 1967 [11] | $C1$ | OH | 24.633 | 14.290 | 25.412 | 90.06 | 89.86 | 89.91 | 8945 | ? |
| T2, $C_3S$: $T$=680 °C | P | Bigare et al., 1967 [11] | $C1$ | OH | 24.528 | 14.270 | 25.298 | 89.98 | 89.75 | 89.82 | 8854 | ? |
| T1, $C_3S$: $T$=20 °C | P | Bigare et al., 1967 [11] | $C1$ | OH | 24.398 | 14.212 | 25.103 | 89.91 | 89.69 | 89.69 | 8704 | ? |
| | S | Golovastikov et al., 1975 [24] | $P$-1 | | 11.67 | 14.24 | 13.72 | 105.5 | 94.33 | 90 | 2190 | 18 |
| | | | | OH | 12.32 | 7.05 | 25.21 | 89.95 | 90.41 | 89.66 | 2190 | |
| | P | de Noirfontaine et al. [35,44] | | OH | 12.307 | 7.041 | 25.097 | 89.74 | 90.23 | 89.7 | 2175 | |

The "S" and "P" letters stand for single crystal or powder diffraction data, respectively. The "H" and "OH" notations refer to (pseudo)hexagonal and (pseudo)orthohexagonal sets of unit cell parameters. In the rhombohedral $R3m$ space group, they are threefold or sixfold unit cells. For the non-rhombohedral polymorphs, they are related to pseudo-symmetries.

[24] (space group $P\bar{1}$; $a$=11.67 Å, $b$=14.24 Å, $c$=13.72 Å, $\alpha$=105.5°, $\beta$=94.33°, $\gamma$=90°), after an impressive work also based upon Weissenberg method. Three types of hexagonal planes were discussed, with one type of Ca-polyhedron per layer.

Ten years later, thanks to automatic four-circle diffractometry, things became much easier than with the pioneering Weissenberg experiments: within a couple of years the structures of two new polymorphs were resolved.

The R structure (space group $R3m$) was resolved quite simultaneously by Nishi and Takéuchi [25] ($a$=7.1350 Å, $c$=25.586 Å) and by Il'inets and Malinovskii [26] ($a$=7.0567 Å, $c$=24.974 Å). Nishi and Takéuchi [25] proposed a model very similar to the average unit cell proposed by Jeffery [9], but they introduced two orientations[4] of the $SiO_4$ tetrahedra, Up and Down, with respect to the pseudo-hexagonal $\mathbf{c}_H$ axis. Except for the silicate orientation, they also showed that their structure was similar to the arrangement found by Golovastikov in the low temperature polymorph.

At the same time, Il'inets and Malinovskii [26] proposed another structure determination of the R form, with a discussion focused on the arrangements of the calcium polyhedra.

A complex model (space group $Cm$; $a$=33.083 Å, $b$=7.027 Å, $c$=18.499 Å, $\beta$=94.12°) was also proposed by Nishi et al. for the M3 polymorph [16]. They

[4] In Jeffery's model, the three tetrahedra have an Up configuration, and their orientations only differ by a rotation of one of them around the threefold axis.

described a large superstructure of an average monoclinic unit cell, referred to as ⟨M⟩ ($a$=12.242 Å, $b$=7.027 Å, $c$=9.250 Å, $\beta$=116.04°), with three types of split (i.e. disordered) ions: calcium ions in special positions, calcium ions in general positions, isolated oxygen ions. This superstructure is described in terms of the same Up and Down orientations of the silicate tetrahedra than in their R structure analysis, but with additional ill-defined G–gauche–orientations.

Simultaneously, some relations between several unit cells were obtained by transmission electron microscopy (TEM) experiments. It is important to underline that using the results from the literature is not a straightforward task due to a mixture of both reverse and obverse conventions in hexagonal setting, and various matrix definitions[5]. Hudson and Groves [29] confirmed the relationship between the large monoclinic unit cell of Jeffery (the M3 polymorph) and the pseudo-hexagonal unit cell. Sinclair and Groves [30] determined a transformation matrix between the T1 structure of Golovastikov et al. [24] and the (pseudo)hexagonal unit cell.

Ten years later, Mumme [31] determined the structure of a crystal of alite, extracted from a clinker, by Weissenberg and four-circle diffractometry experiments (space group *Cm*; $a$=12.235 Å, $b$=7.073 Å, $c$=9.298 Å, $\beta$=116.31°). He described a unit cell similar to the ⟨M⟩ unit cell of Nishi et al. [16], but an important difference was that no superstructure lines were observed.

At that time, both the lowering cost of the laboratory diffraction instruments and the availability of widely distributed and well documented Rietveld-like analysis software made it possible to use this method as an alternative method for an industrial quantitative analysis of clinkers. The most frequent polymorphs found in clinkers are the M3, M1 and sometimes T1 polymorphs. For the M3 polymorph, the Nishi et al. and Mumme models have been tested in many studies [31–37] using standard laboratory equipment available in an industrial context. For the M1 polymorph, a model was proposed by de Noirfontaine et al. [35–39] (space group *Pc*; $a$=27.8736 Å, $b$=7.0590 Å, $c$=12.2575 Å, $\beta$=116.03°). Its application to industrial clinkers will be described in a forthcoming paper.

At the same time, other authors used large instruments such as neutron reactors or synchrotrons to investigate simpler models than the very complicated alite structural model of Nishi et al.

Using neutron powder diffraction data of a synthetic alite, Berliner et al. [40] have shown that the splitting of two types of calcium ions can be neglected without important changes, with the number of independent sites decreasing from 226 to 190. Very recently, de la Torre et al. [41] used high resolution synchrotron X-ray powder diffraction and high resolution neutron powder diffraction data to find a model without splitting for the calcium ions in special positions and the isolated oxygen ions, with a decrease of the independent sites from 226 to 155: the simplified model and the model of Nishi et al. led to similar Rietveld refinements as well in synthetic alite as in industrial clinkers.

A parallel approach is the analysis of the various polymorphs in terms of superstructures with the determination of propagation vectors related to a given average unit cell. Many studies can be found. Urabe et al. [42,43] were able to interpret the diffraction patterns of triclinic and monoclinic polymorphs by TEM investigation in terms of superstructures of a pseudo-hexagonal subcell. At the same time, a propagation vector was determined for the M3 superstructure related to the ⟨M⟩ subcell [33,35,36,44].

Superstructure relations between the T1, M1 and M3 polymorphs have been recently proposed, together with a structural model for the M1 polymorph determined on the basis of powder X-ray diffraction data [35,38,39].

In short, no structural model is still available for the T2, T3 and M2 polymorphs. Various models are available for the T1, M1, M3 and R polymorphs. Two distinct approaches can be found in literature:

- a structural approach, aiming to investigate the atomic structure of the polymorphs and to understand the relations between the polymorphs.
- an approximate approach within the industrial context of Rietveld refinement of powder diffraction data of clinkers. A popular idea is to simplify the exact structural models in order to reduce the number or refined parameters. One can either average the disordered atomic positions or use smaller averaged unit cells.

The metric relations between the conventional unit cells of the known polymorphs cannot be easily related to an underlying common average structure, especially for the Golovastikov unit cell of the T1 polymorph. The following section is devoted to a detailed discussion of the metric relation between the various unit cells found in the literature, in order to relate the triclinic T1 polymorph to the other polymorphs by using unit cells easier to handle than the Golovastikov unit cell.

## 3. Superstructure relations between the polymorphs

Looking throughout the known polymorphs, three distinct elementary blocks must be considered, each of them being related to a given symmetry.

In the following, we shall name $\hat{\mathbf{a}}$ the unit vector parallel to a vector $\mathbf{a}$.

[5] For example, in his paper, p. 50, Ordway [27] gave the relation between M and H bases, but the relation used between the R and H bases [28] was related to a R3 reverse transformation, which is different from that used by Jeffery (reverse R1).

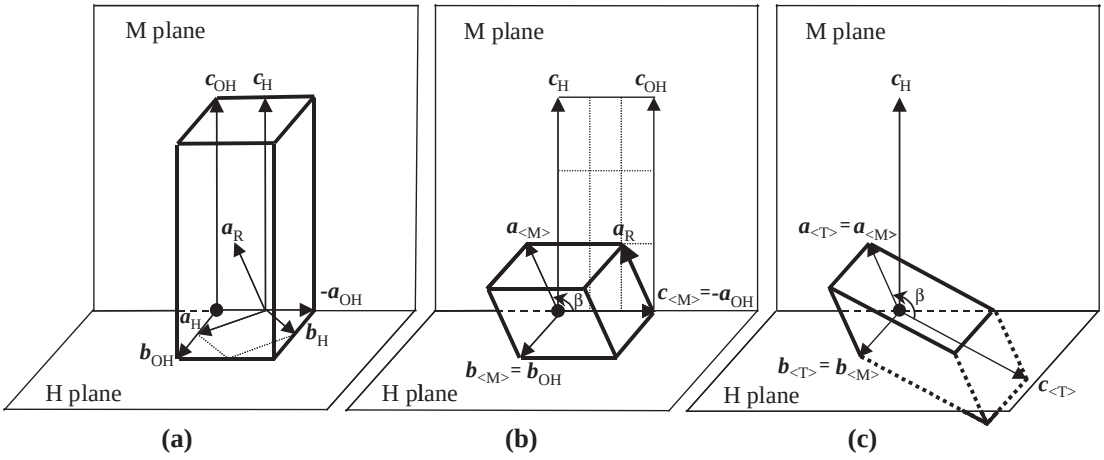


Fig. 1. Hexagonal and monoclinic planes (H and M planes) related to the unit cells of the literature. (a) Unit cell vectors associated to the pseudo-rhombohedral symmetry: rhombohedral R, hexagonal H and orthohexagonal OH unit cells. $V_{OH}=2V_H$; $V_H=3V_R$. (b) Average monoclinic ⟨M⟩ unit cell of Nishi et al., related to the orthohexagonal and rhombohedral unit cell vectors. The rhombohedral $\mathbf{a}_R$ vector is located in the monoclinic plane. The dotted lines illustrate the construction given by Nishi et al. [16]. (c) Average triclinic ⟨T⟩ unit cell, related to the ⟨M⟩ and rhombohedral unit cell vectors.

### 3.1. Three symmetries and three elementary blocks

As shown by Fig. 1 three important symmetry elements appear, each of them being related to a given symmetry: the rhombohedral axis, the hexagonal plane and the monoclinic plane. These planes, referred to as the hexagonal (H) and monoclinic (M) planes are orthogonal to the hexagonal and monoclinic vectors $\mathbf{c}_H$ and $\mathbf{b}_{\langle M\rangle}$, respectively.

#### 3.1.1. High temperature rhombohedral polymorph R

Two types of non-primitive unit cells are usually preferred to the rhombohedral unit cell (Fig. 1a): the threefold hexagonal unit cell (H) and the sixfold orthohexagonal unit cell (OH), which is nothing but a body centred orthorhombic unit cell with a ratio $a_{OH}/b_{OH}=\sqrt{3}$. Both the pseudo-hexagonal and the pseudo-orthohexagonal unit cells have been used by Regourd et al. to describe the deformation of the less symmetric polymorphs on the basis of their powder X-ray diffraction data already mentioned.

#### 3.1.2. Monoclinic polymorphs M3 and M1: the ⟨M⟩ elementary block

Jeffery and later Nishi et al. have shown the persistence of the directions $\hat{\mathbf{a}}_R$ and $\hat{\mathbf{b}}_{OH}$ as unit cell vectors and the direction $\hat{\mathbf{a}}_{OH}$ as the diagonal of the basis of the monoclinic M3 polymorph: $\mathbf{c}_{M3}=2\mathbf{a}_R$, $\mathbf{b}_{M3}=\mathbf{b}_{OH}$ and $\mathbf{a}_{M3}+\mathbf{c}_{M3}=3\mathbf{a}_{OH}$. Nishi et al. first introduced the small averaged unit cell ⟨M⟩ (Fig. 1b) of the M3 large unit cell, also found by Mumme, with a volume $V_{\langle M\rangle}=V_{M3}/6=2V_R$. They gave the metric relationship between the rhombohedral and monoclinic unit cells: Jeffery for the M3 unit cell and Nishi et al. for the ⟨M⟩ unit cell. De Noirfontaine et al. have recently shown that a similar average unit cell ⟨M⟩, but with a distinct space group, can also be introduced as an averaged unit cell for the three times larger M1 polymorph unit cell.

Table 4
Unit cell parameters of our M3, M1 and T1 samples

| Sample | | $a$ (Å) | $b$ (Å) | $c$ (Å) | $\alpha$ (°) | $\beta$ (°) | $\gamma$ (°) | $V$ (Å$^3$) |
|---|---|---|---|---|---|---|---|---|
| M3 | M 3: 6⟨M⟩*Cm* choice 1 | 33.0577 | 7.0330 | 18.5179 | | 94.18 | | 4294 |
| M3 | M′3: 6⟨M⟩*Im* choice 3 | 18.5179(10) | 7.0330(4) | 36.694(19) | | 116.038(4) | | 4294 |
| M3 | ⟨M⟩*Am* average | 9.259 | 7.0330 | 12.231 | | 116.04 | | 716 |
| M1 | M 1: 3⟨M⟩*Pa* choice 1 | 12.2575 | 7.059 | 25.0462 | | 90.06 | | 2167 |
| M1 | M′1:3⟨M⟩*Pc* choice 2 | 27.8736(2) | 7.0590(5) | 12.2575(8) | | 116.030(6) | | 2167 |
| M1 | ⟨M⟩*Pc* average | 9.2912 | 7.059 | 12.2575 | | 116.03 | | 722 |
| T1 | G | 11.631 | 14.2115 | 13.688 | 105.32 | 94.56 | 89.84 | 2175 |
| T1 | G′ | 18.389 | 14.2115 | 17.243 | 102 | 76.93 | 39.23 | 2175 |
| T1 | 3G′: 9⟨T⟩$P\bar{1}$ | 27.909(1) | 21.123(1) | 18.390(1) | 90.390(2) | 143.000(2) | 89.630(2) | 6524 |
| T1 | ⟨T⟩$P\bar{1}$ | 9.303 | 7.041 | 18.39 | 90.39 | 143 | 89.63 | 725 |

For each sample, the various unit cells discussed in the main text (equivalent or averaged unit cells) are given.

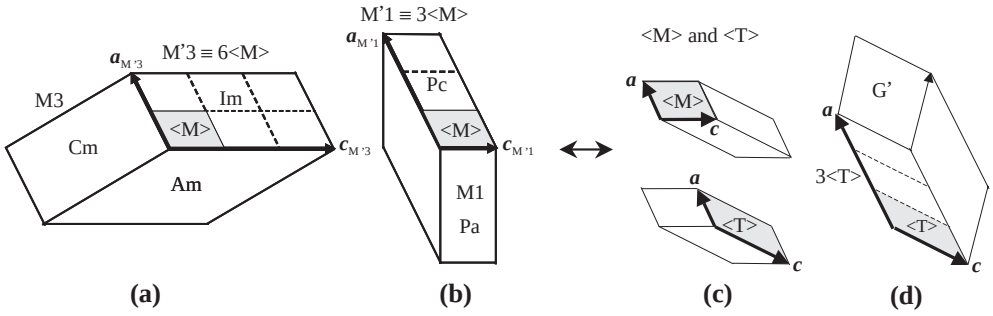


Fig. 2. The monoclinic plane. ⟨M⟩ and ⟨T⟩ elementary blocks and superstructure relationships between the $C_3S$ polymorphs discussed in the text. Tripling the unit cell along the **b** vector transforms the unit cell 3⟨T⟩ into 9⟨T⟩ (3G′).

Things become easier if one introduces some change in the notation of the cell axes, by reversing the **a** and **c** axes of the unit cell with respect to the notation of Nishi et al. [16] and Mumme [31][6].

Within this notation, $\mathbf{a}_{\langle M\rangle}=\mathbf{a}_R$, $\mathbf{a}_{\langle M\rangle}=\mathbf{b}_{OH}$ and $\mathbf{c}_{\langle M\rangle}=-\mathbf{a}_{OH}$.

### 3.1.3. Triclinic polymorph T1: the ⟨T⟩ elementary block

Let us call G the unit cell introduced by Golovastikov et al. [24] for the T1 polymorph. De Noirfontaine et al. [35,38,39] have shown the possibility to introduce an average unit cell ⟨T⟩ of the triclinic unit cell in the following way (Fig. 1c): starting from another triclinic unit cell, G′ equivalent to the Golovastikov unit cell G, then introducing three centring translations, a non-primitive threefold unit cell, 3G′, is found with $V_{3G'}=3V_G$ (Table 4). The most interesting result is that this 3G′ unit cell is pseudo-monoclinic with two unit cell vectors parallel to directions $\hat{\mathbf{a}}_R$ and $\hat{\mathbf{b}}_{\langle M\rangle}$ and the third vector lying in the monoclinic plane: $\mathbf{a}_{3G'}=3\mathbf{a}_{\langle M\rangle}$, $\mathbf{b}_{3G'}=3\mathbf{b}_{\langle M\rangle}$, and $\mathbf{c}_{3G'}=\mathbf{c}_{\langle M\rangle}-\mathbf{a}_{\langle M\rangle}$. The relationship with the previous unit cell ⟨M⟩ seems clear. Introducing the unit cell ⟨T⟩ defined by $\mathbf{a}_{\langle T\rangle}=\mathbf{a}_{\langle M\rangle}$, $\mathbf{b}_{\langle T\rangle}=\mathbf{b}_{\langle M\rangle}$ and $\mathbf{c}_{\langle T\rangle}=\mathbf{c}_{\langle M\rangle}-\mathbf{a}_{\langle M\rangle}$, one finally finds this ⟨T⟩ unit cell to be an averaged unit cell of the 3G′ non-primitive unit cell, with $V_{\langle T\rangle}=V_{3G'}/9=V_G/3$ (note that $\mathbf{c}_{\langle T\rangle}=-\mathbf{a}_{\langle M\rangle}-\mathbf{b}_{\langle G\rangle}$). One recognises between the ⟨T⟩ and ⟨M⟩ unit cells the same relationships than between two equivalent monoclinic unit cells (Fig. 2c).

## 3.2. Elementary blocks and superstructures

### 3.2.1. Metric relations and space groups

Jeffery [9] first introduced some metric relations between his M3 averaged rhombohedral pseudo-structure and the M3 unit cell. Nishi et al. [16] later introduced the atomic positions in the M3 unit cell and introduced the ⟨M⟩ averaged unit cell. The superstructure becomes more evident using another choice for the monoclinic unit cell, i.e. non-conventional unit cells ⟨M⟩ and M′3 (Fig. 2a; Table 4).

$$M'3 \equiv 6\langle M\rangle \equiv (2,1,3)\langle M\rangle$$

Here the notation $n\langle M\rangle$, where $n$=pqr, stands for (p,q,r)⟨M⟩ as a condensed notation for a ($p\mathbf{a}_{\langle M\rangle}$, $q\mathbf{b}_{\langle M\rangle}$, $r\mathbf{c}_{\langle M\rangle}$) supercell of ⟨M⟩.

De Noirfontaine et al. [35,38,39] have shown a similar situation (Fig. 2b; Table 4) for the M1 polymorph by XRD and TEM:

$$M'1 \equiv 3\langle M\rangle \equiv (3,1,1)\langle M\rangle$$

Here the M′1 unit cell is equivalent to the M1 pseudo-orthohexagonal monoclinic unit cell introduced by Regourd et al. [11,12].

The case of the triclinic T1 polymorph is similar when referring to the non-primitive 3G′ unit cell described above (Fig. 2d):

$$3G' \equiv 9\langle T\rangle \equiv (3,3,1)\langle T\rangle$$

At this stage, three elementary blocks are highlighted, with distinct shapes. Various superstructures can be derived, sometimes using non-conventional unit cells in order to clarify the superstructure relationships. But for a given shape[7] of the elementary block (e.g. ⟨M⟩ or ⟨T⟩), the content of the unit cell varies from one polymorph to another. This content is defined by the asymmetric unit of the true unit cell (e.g. 6⟨M⟩ or 9⟨T⟩) and the space group (e.g. *Cm* or $P\bar{1}$) which generates the remaining atoms of the unit cell by acting on the content of the asymmetric unit.

Therefore, the various models can be labelled by combining the shape of the unit cell (i.e $6\langle M\rangle \equiv (2,1,3)\langle M\rangle$)

[6] The choice of the axes in ⟨M⟩ unit cells of Nishi et al. [16] and of Mumme [31] (conventional cells with $a>c$) leads to a vector **b** in the direction opposite to the vector **b** of M3 ($\mathbf{b}_{\langle M\rangle}=-\mathbf{b}_{M3}$). Throughout all this paper, we chose to swap the **a** and **c** axes of ⟨M⟩: then $\mathbf{b}_{\langle M\rangle}=\mathbf{b}_{M3}$. With this convention, the cell parameters of the ⟨M⟩ average structure of Nishi et al. becomes: $a$=9.250 Å, $b$=7.027 Å, $c$=12.242 Å, $\beta$=116.04°, and those of ⟨M⟩ unit cell of Mumme: $a$=9.298 Å, $b$=7.073 Å, $c$=12.235 Å, $\beta$=116.31°. This permutation transforms the *Cm* space group into *Am*.

[7] Here "shape" has to be understood as a rather general word neglecting the small variation of the cell parameters, such as a triclinisation of the unit cell. The two "shapes" to be considered here are given by Fig. 1b and c.

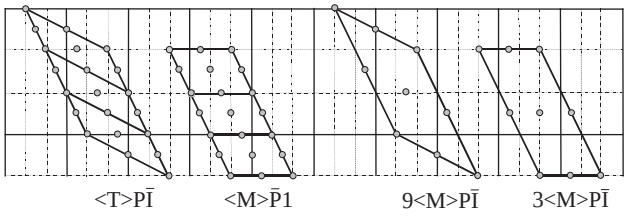


Fig. 3. $P\bar{1}$ space group: conservation of inversion centres in the ⟨M⟩ and ⟨T⟩ unit cells, but not in the 3⟨M⟩ and 9⟨T⟩ unit cells.

⟨M⟩) and the space group (i.e. *Im*), which depends on the choice of the unit cell axes: conventional or equivalent non-conventional unit cell (i.e. *Cm* or *Im*).

Within these notations, the known structures of the polymorphs can be written:

M3 polymorph: 6⟨M⟩*Im* or 6⟨M⟩*Cm* within Nishi et al. conventional choice
Mumme sample: ⟨M⟩*Am* or ⟨M⟩*Cm* within Mumme conventional choice
M1 polymorph: 3⟨M⟩*Pc*
T1 polymorph: 9⟨T⟩$P\bar{1}$ Fig. 3 states that ⟨T⟩$P\bar{1}$ ≡⟨M⟩$P\bar{1}$

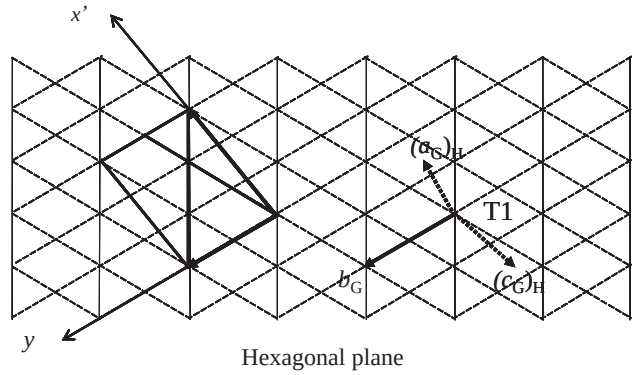


Fig. 5. Link between our Fig. 4 and Fig. 1 of Golovastikov et al.'s paper [24]. The coordinates $x'$ and $y$ are taken along the directions $\mathbf{a}_G$–$\mathbf{c}_G$ and $\mathbf{b}_G$, respectively.

Fig. 4 summarises the different unit cells, either conventional or non-conventional, either taking or not taking the superstructures into account. The link between our Fig. 4 and Fig. 1 of Golovastikov et al. [24] is given by Fig. 5.

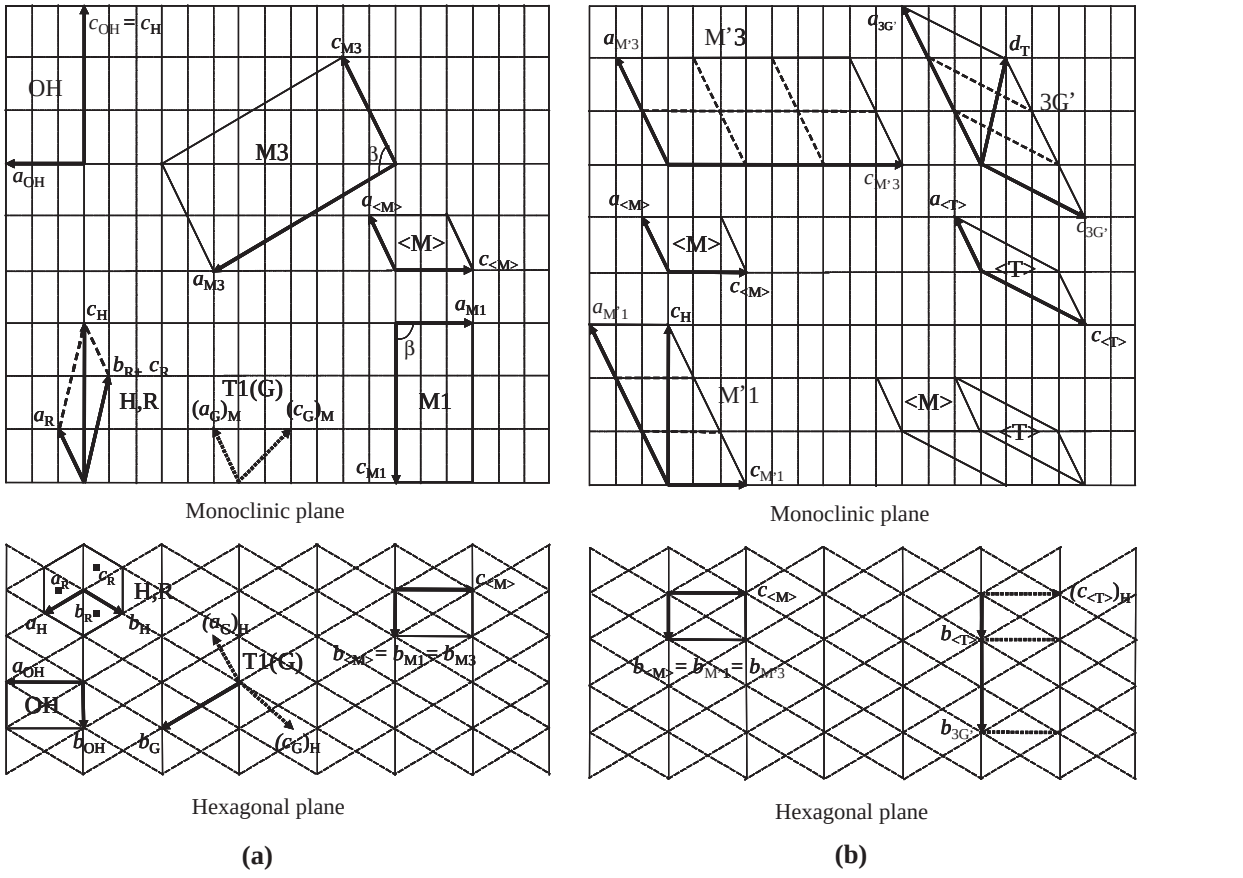


Fig. 4. Projections of the unit cells of the various polymorphs onto the hexagonal and monoclinic planes. All the axes are chosen in such a way that the monoclinic axes ($\mathbf{b}_i$) are parallel to the same direction. (a) Unit cells as defined in the literature: R rhombohedral, H hexagonal, OH orthohexagonal; M1, M3, ⟨M⟩ monoclinic; T1(G) triclinic as introduced by Golovastikov et al. For the T1(G) unit cell, $(\mathbf{a}_G)_H$, $(\mathbf{c}_G)_H$, $(\mathbf{a}_G)_M$ and $(\mathbf{c}_G)_M$ are the projections of the cell basis vectors onto the hexagonal H and monoclinic M planes. (b) The various monoclinic and triclinic unit cells, most of them non-conventional, introduced in the text.

*3.2.2. Experimental evidence: propagation vectors*

The extensive TEM studies made by Urabe et al. [42,43] aimed at finding–in a systematic way and for all the polymorphs–some propagation vectors related to a hexagonal averaged unit cell. Starting from XRD data, Courtial et al. [44] gave another propagation vector for M3, related to the ⟨M⟩ averaged unit cell.

Whatever the experimental technique, TEM or XRD, the superstructures produce additional weak characteristic Bragg lines. The case of the monoclinic polymorphs was discussed by Courtial et al. [44]: five angular windows are introduced, among which two were discussed since the 1960s in the literature (Regourd et al. [11,13]). They contain all the significant Bragg lines characteristic of such polymorphs.

One can notice that the two average structures $3\langle T\rangle P\bar{1}\equiv(3,1,1)$ $\langle T\rangle P\bar{1}$ and $\langle T\rangle P\bar{1}$ are both able to reproduce the strongest lines of the X-ray powder diffraction pattern of the triclinic T1 polymorph. But they cannot reproduce the observed fine structure of the triclinic T1 pattern (de Noirfontaine [35]). However, a–triclinic–$\langle T\rangle P\bar{1}$ model with rigid bodies refinement is able to reproduce rather closely the XRD data of the–monoclinic–M1 alite. Despite its lack of physical meaning, it may be used in a phenomenological way for the high temperature triclinic polymorphs T2 and T3 as long as no accurate atomic model is known.

*3.3. Persistence of the rhombohedral directions and common repeats*

It is interesting to note the persistence of the four main directions and distances (or their multiples) found in the rhombohedral unit cell throughout the various polymorphs (Table 5).

The direction of the rhombohedral unit cell vector $\mathbf{a}_R$ is always found:

$$\mathbf{a}_R,\quad \mathbf{a}_{\langle M\rangle}=\mathbf{a}_R,\ \mathbf{a}_{M'1}=3\mathbf{a}_R,\quad \mathbf{a}_{M'3}=2\mathbf{a}_R,$$
$$\mathbf{a}_{\langle T\rangle}=\mathbf{a}_R,\quad \mathbf{a}_{3G'}=3\mathbf{a}_R.$$

The two diagonals $\mathbf{b}_R+\mathbf{c}_R$ and $\mathbf{b}_R-\mathbf{c}_R$ of the face of the rhombohedral unit cell do not persist in all the polymorphs:

– the diagonal $\mathbf{b}_R-\mathbf{c}_R=\mathbf{a}_H+\mathbf{b}_H=\mathbf{b}_{OH}=\mathbf{b}_{\langle M\rangle}=\mathbf{b}_{M'1}=\mathbf{b}_{M'3}=\mathbf{b}_{\langle T\rangle}=\mathbf{b}_{3G'}/3$ is always found,

Table 5
Occurrence of the main directions of the rhombohedral unit cell in the known polymorphs

| | $\mathbf{a}_R$ | $\mathbf{b}_{\langle M\rangle}=\mathbf{b}_R-\mathbf{c}_R$ | $d_T=\mathbf{b}_R+\mathbf{c}_R$ | $\mathbf{c}_H=\mathbf{a}_R+\mathbf{b}_R+\mathbf{c}_R$ |
|---|---|---|---|---|
| R, H, OH | × | × | | × |
| M3 | × | × | | |
| M1 | × | × | | × |
| T1 | × | × | × | |

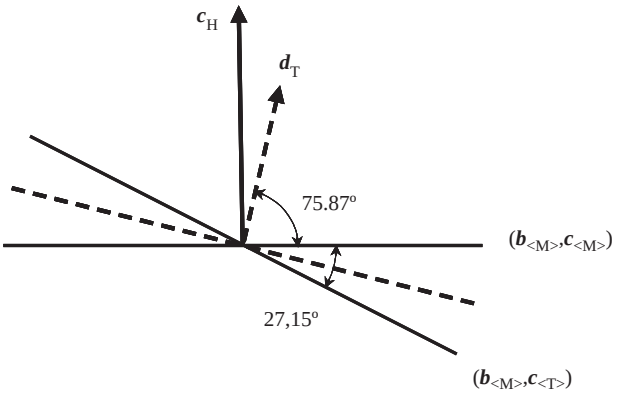


Fig. 6. Orientation of the pseudo-repeat $d_T$=17.33 Å discussed by Golovastikov et al. with respect to the basal planes of the ⟨M⟩ and ⟨T⟩ unit cells. The angle 80°45′ mentioned in their paper seems irrelevant: the proper value is 75.87°.

– but the diagonal $\mathbf{b}_R+\mathbf{c}_R=\mathbf{a}_{3G'}+\mathbf{c}_{3G'}=\mathbf{a}_G+\mathbf{c}_G$ located in the monoclinic plane is only found in the triclinic polymorph, and therefore referred to as $d_T$.

The body diagonal $\mathbf{a}_R+\mathbf{b}_R+\mathbf{c}_R=\mathbf{c}_H=\mathbf{c}_{OH}=\mathbf{c}_{M1}=\mathbf{a}_{M'1}+\mathbf{c}_{M'1}$ disappears in the monoclinic M3 and the triclinic T1 polymorph.

A rotation from the hexagonal or pseudo-hexagonal direction $\mathbf{c}_H$ related to the trigonal symmetry or pseudo-symmetry to the $d_T$ pseudo-hexagonal direction occurs when passing from the monoclinic to the triclinic symmetry. As sketched by Fig. 6, $d_T$ is normal to a plane roughly intermediate between the monoclinic basal plane $(\mathbf{b}_{\langle M\rangle},\mathbf{c}_{\langle M\rangle})$ and the triclinic basal plane $(\mathbf{b}_{\langle M\rangle},\mathbf{c}_{\langle T\rangle})$.

In the conclusion of their paper, Golovastikov et al. [24] already explained that the common repeat $\mathbf{c}_H$=25.29 Å is related to a 10-layer stacking whereas the common repeat $d_T$=17.33 Å is related to a 7-layer stacking, with a lateral shift of the layers. In the next paragraph, we discuss the link between these important directions and planes and the structural elements.

## 4. Persistence of 1D and 2D structural elements and their link with observed properties

*4.1. Polymorphism and average unit cell*

Regourd and co-workers [11] determined the displacive type of the transformations on the basis of their metric work (dimensions and symmetries of the various lattices). The authors discussed the evolution of the cell parameters of a same pseudo-hexagonal or ortho-hexagonal unit cell refined on the X-ray powder diffraction data of all the polymorphs.

The true structures introduced later confirmed the existence of a persistent average unit cell. An approximate structure can be built starting from the known T1, M1 and M3 structures interpreted as superstructures of ⟨T⟩ and ⟨M⟩

Table 6
Approximate fractional positions of the atoms of the average unit cell ⟨M⟩*Am*

| | | | |
|---|---|---|---|
| $Si_1$: 0 0 0 | $Si_2$: 2/3 0 1/4 | $Si_3$: 1/3 0 3/4 | (0,1/2,1/2)+ |
| $Ca_4$: 2/3 0 3/4 | $Ca_5$: 1/3 0 1/4 | $Ca_6$: 0 0 1/2 | (0,1/2,1/2)+ |
| $O_2$: 1/2 0 1/2 | $O_7$: 7/8 0 5/8 | $O_8$: 1/8 0 3/8 | (0,1/2,1/2)+ |
| $Ca_1$: 1/3 1/4 0 | $Ca_2$: 2/3 1/4 0 | $Ca_3$: 0 1/4 1/4 | (0,1/2,1/2)+ |
| | | | (0,0,1/2)+ |

The oxygen ions of the silicates are not given, due to the orientational disorder of the tetrahedra. The numbering of the atoms is that of the Mumme structural model [31]. The translations given in the last column are used to generate the other atoms.

average unit cells, with a subsequent transformation from the ⟨T⟩ to a ⟨M⟩ equivalent (pseudo-monoclinic) unit cell. The differences consist in small displacements of calcium atoms and changes in the orientational order or disorder of the $SiO_4$ tetrahedra [35,38]. The local deformations become more and more important when passing from rhombohedral to triclinic symmetry. In this ⟨M⟩ average structure, the positions of the atoms are always close to simple fractional values (Table 6), except for the oxygen of the tetrahedra. In what follows, we consider only the central silicon ion positions. Persistent 1D and 2D structural objects can now be introduced.

### 4.2. Persistent 1D and 2D structural elements

#### 4.2.1. Layers and chains

Looking at the atomic content of the planes introduced in Section 3.1, three hexagonal planes $H_1$, $H_2$, $H_3$ ($x$=0, 2/3, 1/3) and four monoclinic planes $M_0$, $M_{1/4}$, $M_{1/2}$, $M_{3/4}$ ($y$=0, 1/4, 1/2, 3/4) have to be considered.

The calcium polyhedra are organised in three families of hexagonal layers ($\mathbf{b}_{\langle M\rangle}$, $\mathbf{c}_{\langle M\rangle}$), the $H_1$, $H_2$, $H_3$ layers of Fig. 7a,b, discussed by Il'inets and Malinovskii [26] and Golovastikov et al. [24] for the R and T1 polymorphs.

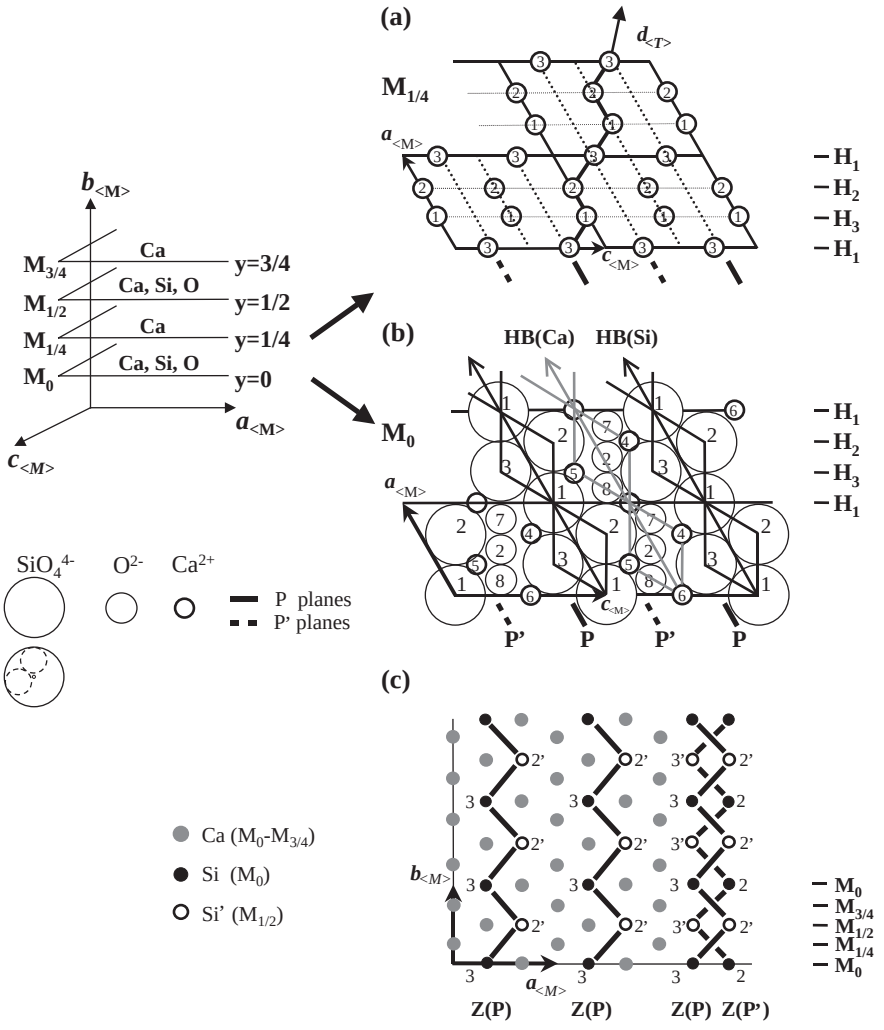


Fig. 7. Structural elements associated with the monoclinic symmetry. (a, b) The two families of alternate monoclinic layers. The mixed layers ($M_0$ and $M_{1/2}$) contain silicate, calcium and isolated oxygen ions. The other layers ($M_{1/4}$ and $M_{3/4}$) only contain calcium ions. (a) Monoclinic layers $M_{1/4}$ and $M_{3/4}$: zigzag chains of calcium along the $d_T$ direction. (b) Monoclinic layers $M_0$ and $M_{1/2}$: herringbone-like chains (HB) along the rhombohedral axis $\mathbf{a}_R$=$\mathbf{a}_{\langle M\rangle}$. (c) Zigzag chains of silicates. Z(P) and Z(P′) are zigzag chains, located in the P and P′ planes, respectively. The P and P′ planes are parallel ($\mathbf{a}_{\langle M\rangle}$,$\mathbf{b}_{\langle M\rangle}$) planes as sketched in (a,b). The big circles are the envelopes of the silicates.

Table 7
Average distances between silicon ions in R [25], ⟨M⟩ [31], M3 [16], M1 [39] and T1 [24] known structural models

| | Type of distances | R | ⟨M⟩ | M3 | M1 | T1 |
|---|---|---|---|---|---|---|
| $d_P$ (Å) | $Si_2$–$Si_3$ | 4.79 | 4.75 | 4.79 | 4.81 | 4.84 |
| $d_{ZA}$ (Å) | $Si_2$–$Si_3$ | 4.79 | 4.77 | 4.74 | 4.84 | 4.80 |
| $d_T$ (Å) | $Si_1$–$Si_{2,3}$ | 5.11 | 5.04 | 5.03 | 4.99 | 5.05 |
| $d_{ZB}$ (Å) | $Si_1$–$Si_{2,3}$ | 5.11 | 5.02 | 5.01 | 5.01 | 5.01 |
| $d_H$ (Å) | $Si_1$–$Si_{2,3}$ | 5.49 | 5.40 | 5.39 | 5.46 | 5.45 |
| $d_{IH}$ (Å) | $Si_2$–$Si_3$ | 7.34 | 7.14 | 7.13 | 7.10 | 7.20 |
| $d_{IZ}$ (Å) | $Si_2$–$Si_3$ | 7.34 | 7.16 | 7.13 | 7.07 | 7.18 |
| $\Delta\theta_H$ (°) | | 0 | 0.67 | 1.63 | 3.63 | 3.27 |
| $\Delta\theta_T$ (°) | | 0.69 | 0.21 | 1.71 | 2.99 | 2.85 |
| $\theta_P$ (°) | | 53.22 | 54.48 | 54.53 | 54.68 | 54.69 |

The distances and angles are defined at Fig. 8. $d_{ZA}$, $d_{ZB}$ and $d_{IZ}$ are respectively related to $d_P$, $d_T$ and $d_{IH}$ by the pseudo-ternary axis parallel to $d_H$ and $\mathbf{c}_H$. $d_{IH}$ and $d_{IZ}$ are inter-herringbones and inter-zigzag distances.

One observes an alternation of monoclinic layers, the $M_0$, $M_{1/4}$, $M_{1/2}$, $M_{3/4}$ layers of Fig. 7a, described by Nishi et al. in the R and M3 polymorphs. They contain either calcium ions only (the $M_{1/4}$ and $M_{3/4}$ layers related by the $\mathbf{b}_H$ pseudo-translation) or a mixture of calcium, silicate and isolated oxygen ions (the $M_0$ and $M_{1/2}$ layers related by the same $\mathbf{b}_H$ pseudo-translation).

Silicate and calcium ions are organised in three types of chains: herringbone-like chains of silicate or calcium ions (HB(Si) and HB(Ca) in Fig. 7b) along the **a** axes ($\mathbf{a}_R=\mathbf{a}_{\langle M\rangle}=\mathbf{a}_{\langle T\rangle}$), zigzag chains of calcium ions along the $d_T$ diagonal (Fig. 7a), and zigzag chains of silicate ions along the **b** monoclinic axes ($\mathbf{b}_{\langle M\rangle}=\mathbf{b}_{\langle T\rangle}=\mathbf{a}_H+\mathbf{b}_H$) (Z in Fig. 7c) [35,36,38]. Two consecutive silicate ions in a zigzag chain belong to two adjacent $H_2$ and $H_3$ hexagonal sheets and to two distinct herringbone-like chains of the monoclinic layers.

As shown in the previous paragraph (Table 5), the **a** and **b** directions associated with the silicates chains are important directions in all the polymorphs, which is not the case for the $d_T$ and $\mathbf{c}_H$ directions.

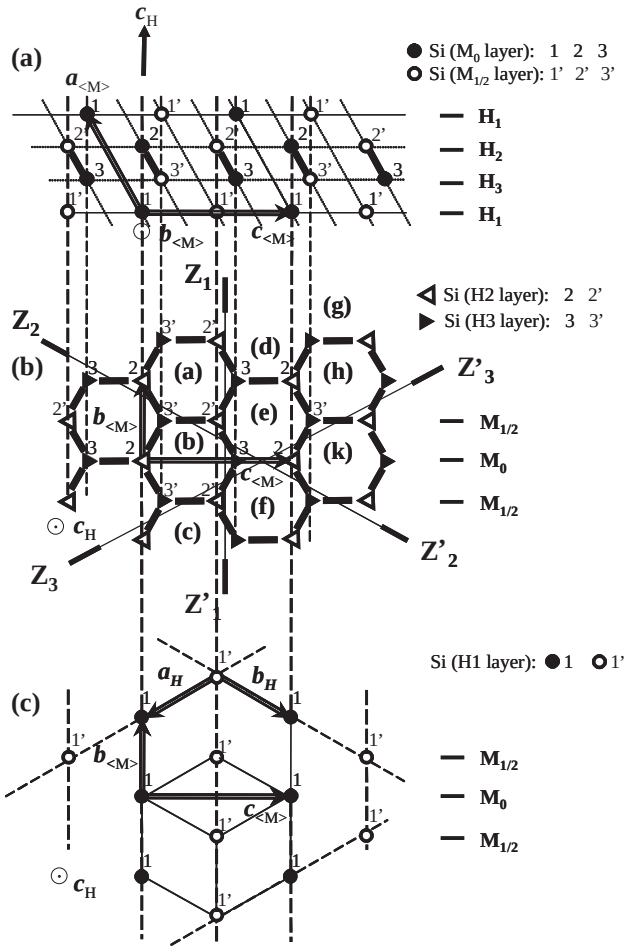


Fig. 9. Layout of the three families of zigzag connected by the ternary pseudo-symmetry (a and b) and the two families of layers (b and c). The letters between parentheses are the centres of the chair conformation rings of six silicates, also used for Fig. 10, occupied by the triplets of isolated oxygen ions, normal to the layers. (a) Projection of the monoclinic layers $M_0$ and $M_{1/2}$. (b) Projection of the hexagonal layers $H_2$ and $H_3$: the central holes of the hexagons are oblique quasi-cylindrical cavities parallel to the rhombohedral axis $\mathbf{a}_{\langle M\rangle}$; they contain the herringbone-like chains of calcium ions. Note: $d_{Si1-Si1'}\approx d_{Si2-Si2'}\approx d_{Si3-Si3'}\approx a_H\approx b_H\geq 7$ Å are the pseudo-hexagonal unit cell parameters. (c) Projection of the hexagonal H1 layers.

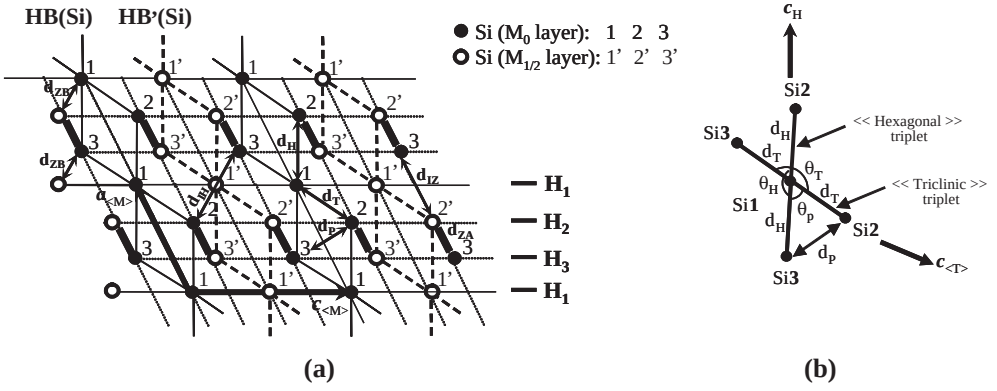


Fig. 8. Definition of the distances and angles of Table 7. (a) Projection of the monoclinic layers $M_0$ and $M_{1/2}$: the thick dashes (2–3′ and 2′–3) are the projections of the zigzag chains along $\mathbf{b}_{\langle M\rangle}$ of Fig 7c. The herringbone-like silicate chains HB(Si) and HB′(Si) are located respectively in the $M_0$ and $M_{1/2}$ layers. The chain HB′(Si) is above the HB(Ca) chain of Fig. 7b. (b) The so-called hexagonal and triclinic silicate triplets are respectively parallel or quite parallel to the hexagonal axis $\mathbf{c}_H$ and quite parallel to the triclinic axis $\mathbf{c}_{\langle T\rangle}$.

*4.2.2. Organisation of the silicon ions*

Averaging the distances between silicon ions in each structure (R, ⟨M⟩, M3, M1 and T1), one observes (Table 7; Fig. 8) three distinct silicon–silicon distances—$d \approx 4.8$ Å for the $Si_2$–$Si_3$ pairs, $d \approx 5$ Å and $d \approx 5.4$ Å for the $Si_1$–$Si_{2,3}$ pairs ($d_T$, $d_{ZB}$, $d_H$)—and then a gap until $d \geq 7$ Å. The shortest $d \approx 4.8$ Å distances link the $Si_2$ and $Si_3$ kinds of atoms in herringbone-like chains ($d_P$) and in zigzag chains ($d_{ZA}$). The largest $d \geq 7$ Å distances include the various lattice translations (hexagonal or monoclinic) observed in the different polymorphs. The gap between 5.4 Å and 7 Å is the result of the organisation in silicate chains, with a clear separation between short intra-chains Si–Si distances and larger inter-chains Si–Si distances.

The chains of silicate ions in the monoclinic layers are made of a herringbone-like combination of two types of silicate triplets respectively parallel to the (pseudo)hexagonal axis $\mathbf{c}_H$ and quite parallel to the triclinic axis $\mathbf{c}_{\langle T \rangle}$ (Fig. 8b), so-called "hexagonal" and "triclinic" triplets. A deformation of these triplets with the polymorph, with both a bending and a pinching (Table 7; Fig. 8b) can be observed. $\Delta\theta_H = 180° - \theta_H$ and $\Delta\theta_T = 180° - \theta_T$ are the bending angles of the two triplets, $\theta_P$ is the pinching angle.

*4.2.3. Organisation of the hexagonal layers*

It is now interesting to look at the distribution of the various $d_{Si-Si}$ distances among the various layers. The three families of zigzag chains (Z1, Z2 and Z3 in Figs. 9 and 10) related by the pseudo-ternary symmetry constitute a 2-D network of first $Si_2$–$Si_3$ neighbours (Fig. 9) which constitute thick hexagonal layers (the set of $H_2$+$H_3$ sheets) containing all the first-neighbour silicate ions. Fig. 10 clearly shows that this thick layer, with a 2D array of cyclohexanic-like rings of six silicates in chair conformation, is similar to the sets of neighbouring (111) sheets of a diamond cubic structure [45].

The holes in the thick layers of Fig. 9 are crossed by the oblique herringbone-chains of calcium of the monoclinic layers of Fig. 7b. These thick layers ($H_2$+$H_3$) are separated by the hexagonal layers $H_1$ containing silicates $Si_1$ only, each of them being located at larger distances from its neighbours ($d_{Si1-Si2,3} \approx 5$ Å). The local order is identical for the ions of the $H_2$ and $H_3$ sheets. It is different for the ions of the $H_1$ sheets due to the out-of-plane stacking of the hexagonal sheet with a lateral shift.

Despite the existence of three hexagonal sheets with an identical chemical content (hexagonal 2D network of silicate and calcium ions), we are led to the idea of only two distinct families of layers.

*4.3. Link with the orientational disorder*

Two $Si_1$–$Si_{2,3}$ distances are related to the herringbone-like chains: $d_T \approx 5$ Å and $d_H \approx 5.4$ Å. The former is related to silicate ions located in adjacent hexagonal layers, whereas the latter is related to silicate ions located in non-adjacent hexagonal layers. For this reason, the reference to the only hexagonal direction $\mathbf{c}_H$ along $d_H$ to define "Up" and "Down"

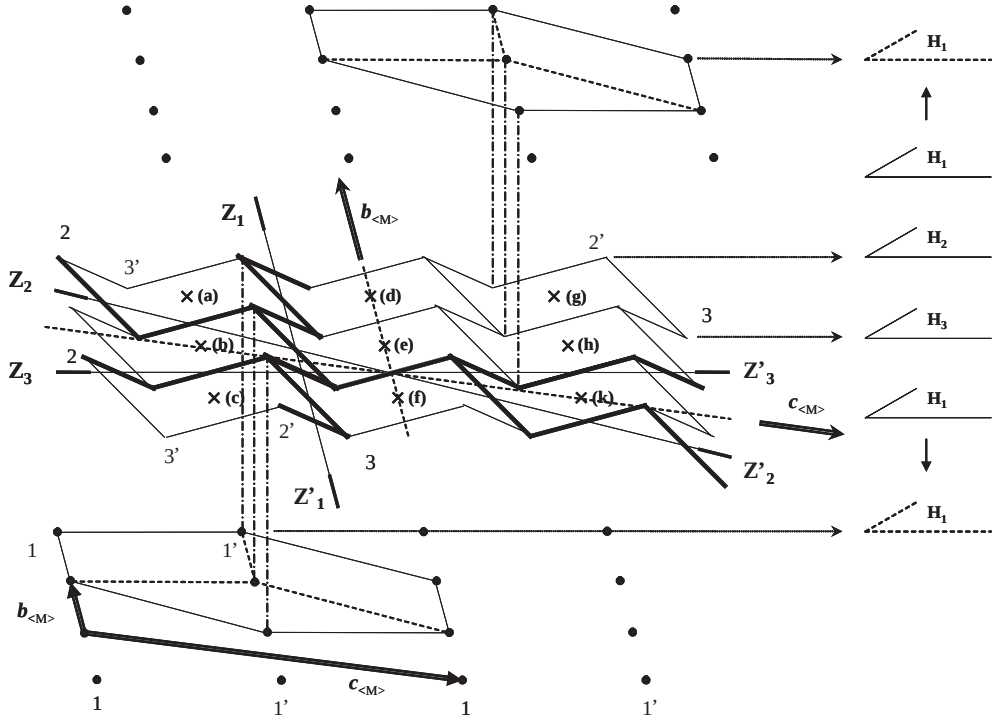


Fig. 10. Split perspective view of the two types of layers H1 and H2+H3. The dotted H1 planes are the splitted positions, and the continuous H1 planes are the real places.

orientations of the silicate ions is not sufficient. One also needs to consider the other direction along $d_T$, i.e. along the triclinic triplets (Fig. 8), with a more physically relevant meaning. Thereby, the ill-defined "G" orientations introduced by Nishi et al. for the M3 polymorph can be interpreted as "Up" and "Down" orientations along the directions of these triclinic triplets.

As shown above, a stacking of two types of silicate layers in the hexagonal direction can be observed.

It is interesting now to connect this discussion with the orientational disorder of the silicate ions. Each type of hexagonal layer is related to a given type of orientational order or disorder (depending on the polymorph):

- the $H_2$+$H_3$ "thick" hexagonal layer (Fig. 11) contains silicate ions with rather simple orientations. They can be described as "Up" or "Down" with respect to the orientation of the hexagonal or triclinic triplets, with gear-like configurations.
- the $H_1$ hexagonal layer contains silicates with more distant silicate neighbours owing to a more complex and frustrated orientational disorder in the high temperature polymorphs.

### 4.4. Link with chemistry: effect of impurities

A systematic study by Maki and co-workers [19,20] of alite crystals found in various clinkers, using X-ray diffraction and optical observations, have shown the correlation between the type and amount of impurity and the stabilised polymorph. Sulphate or magnesium impurities induce the stabilisation of the M1 or M3 polymorphs, respectively.

The structure, as described below, allows an interpretation of some observations in the literature. In M1 alite, the observed superstructure along the axis **a** can probably be ascribed to the substitution of the silicate ions $SiO_4^{4-}$ by sulphate ions $SiO_4^{2-}$. In M3 alite, the observed superstructure in the monoclinic (**a**, **c**) plane can probably be related to a substitution of the calcium ions $Ca^{2+}$ in the calcium-only monoclinic sheets (Fig. 7a). This allows a higher freedom of the position of the calcium and silicate ions along the direction normal to the layer, due to the lack of mirror.

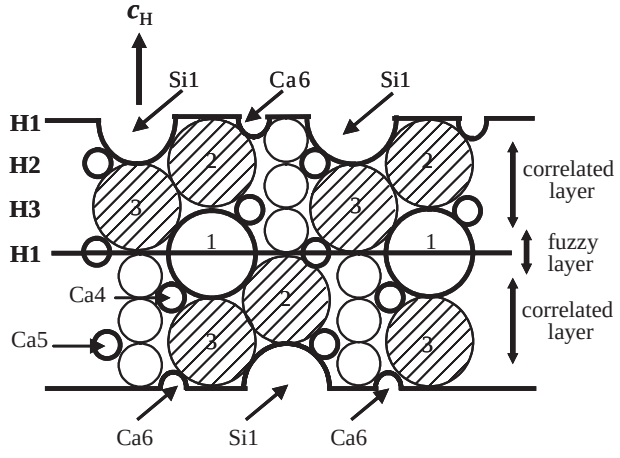


Fig. 11. The two types of layers of silicates: fuzzy layer: $H_1$ hexagonal layer of frustrated and orientationally disorder $Si_1$ silicates; correlated layer: $H_2$+$H_3$ hexagonal layers of gear-like $Si_2$ and $Si_3$ silicates. The cut is along the $M_0$ layer of Fig. 9A.

## 5. Conclusion

The various polymorphs were described in a complex way in the literature. A first complication arises from the description in terms of packing of calcium polyhedra of complex shape. In this paper, we have mainly described the various infinite 1D and 2D structural elements constituting the network of silicates ions. The network of the calcium ions located in the $M_0$ and $M_{1/2}$ monoclinic layers is identical, with a $\mathbf{c}_{\langle M\rangle}/2$ translation. The calcium monoclinic layers $M_{1/4}$ and $M_{3/4}$ located in between have no equivalent silicon network.

Another complication arises from the description in terms of conventional unit cell, which conceals the links between the various unit cells. Using non-conventional and non-primitive unit cells clarifies the relations between the polymorphs:

- The T1, M1, M3 and R polymorphs can be described in terms of superstructures of three related elementary blocks: the R rhombohedral unit cell, the ⟨M⟩ and ⟨T⟩ unit cells.
- The $\mathbf{a}_R$ and $\mathbf{b}_{\langle M\rangle}$ directions are found in all the polymorphs and they are parallel to the 1D chains (zigzag or herringbone-like chains) of silicates or calcium ions.
- The two common repeats, respectively associated to the mean diagonal $\mathbf{c}_H$ of the rhombohedral unit cell and to the diagonal $d_T$ of the basis of the triclinic unit cell, already discussed by Golovastikov et al., are only found in some polymorphs.
- No simple direction seems to correspond to the M3 observed superstructure in which the modulation may be located in the calcium planes, which permit a higher degree of freedom due to the lack of mirror.

The interpretation of the orientational disorder is easier when considering two families of hexagonal layers showing different orientational disorder and two favoured directions parallel to two types of triplets of silicates. We are led with the image of an alternation of thick orientationally "correlated" layers (with a diamond-like conformation of the silicates) separated by more disordered and frustrated layers of graphite-like silicates $Si_1$. We call them "fuzzy" layers. One can wonder whether these "fuzzy" layers constitute the weak points of the structure, responsible for the hexagonal cleavage frequently observed.

## Acknowledgements

The authors warmly thank M. Pierre Jaugey (Ciments CALCIA, France) and Prof. Hélène Zanni (University of Pierre and Marie Curie – ESPCI, France) for their constant support to this work, including financial support, Prof. Micheline Moranville-Regourd for valuable discussions and advice, and Prof. Henri Szwarc for his critical reading of the manuscript.

## References

[1] K.H. Jost, B. Ziemer, R. Seydel, Redetermination of the structure of β-dicalcium silicate, Acta Crystallogr., B 33 (1977) 1696–1700.
[2] W.G. Mumme, R.J. Hill, G. Bushnell-Wye, E.R. Segnit, Rietveld crystal structure refinements, crystal chemistry and calculated powder diffraction data for the polymorphs of dicalcium silicate and related phases, Neues Jahrb. Mineral. Abh. 169 (1995) 35–68.
[3] P. Mondal, J.W. Jeffery, The crystal structure of tricalcium aluminate, $Ca_3Al_2O_6$, Acta Crystallogr., B 31 (1975) 689–696.
[4] F. Nishi, Y. Takéuchi, The $Al_6O_{18}$ rings of tetrahedra in the structure of $Ca_{8.5}NaAl_6O_{18}$, Acta Crystallogr., B 31 (1975) 1169–1173.
[5] A.A. Colville, S. Geller, The crystal structure of brownmillerite, $Ca_2FeAlO_5$, Acta Crystallogr., B 27 (1971) 2311–2315.
[6] A.A. Colville, S. Geller, The crystal structure of $Ca_2Fe_{1.43}Al_{0.57}O_5$ and $Ca_2Fe_{1.28}A_{l0.72}O_5$, Acta Crystallogr., B 28 (1972) 3196–3200.
[7] H.F.W. Taylor, Cement Chemistry, 2nd ed., Thomas Telford Edition, London, 1997.
[8] J.W. Jeffery, Crystal Structure of Tricalcium Silicate and Cobalt Mercury Thiocyanate, PhD thesis No. DX194617, London University (1950).
[9] J.W. Jeffery, The crystal structure of tricalcium silicate, Acta Crystallogr. 5 (1952) 26–35.
[10] J.W. Jeffery, The Tricalcium Silicate Phase, Proc. of the 3rd ISCC, London, vol. 1, 1954, pp. 30–48.
[11] M. Bigaré, A. Guinier, C. Mazières, M. Regourd, N. Yannaquis, W. Eysel, T. Hahn, E. Woermann, Polymorphism of tricalcium silicate and its solid solutions, J. Am. Ceram. Soc. 50 (11) (1967) 609–619.
[12] A. Guinier, M. Regourd, Structure of Portland cement minerals, Proc. of the 5th ISCC, Tokyo, vol. 1, The Cement Association of Japan, Tokyo, 1968, pp. 1–41.
[13] M. Regourd, Polymorphisme du silicate tricalcique. Nouvelles données de la diffraction des rayons X, C. R. Acad. Sci., Sci. Paris Terre 289 (1979) 17–20.
[14] I. Maki, S. Chromy, Microscopic study on the polymorphism of $Ca_3SiO_5$, Cem. Concr. Res. 8 (4) (1978) 407–414.
[15] W. Eysel, T. Hahn, Polymorphism and solid solution of $Ca_3GeO_5$ and $Ca_3SiO_5$, Zeit Krist. 131 (1970) 40–59.
[16] F. Nishi, Y. Takéuchi, I. Maki, The tricalcium silicate $Ca_3O[SiO_4]$: the monoclinic superstructure, Zeit Krist. 172 (1985) 297–314.
[17] T. Hahn, W. Eysel, E. Woermann, Crystal chemistry of tricalcium silicate solid solutions, in: Proc. of the 5th ISCC, Tokyo, vol. 1, 1969, pp. 61–66.
[18] E. Woermann, Th. Hahn, W. Eysel, The substitution of alkalies in tricalcium silicate, Cem. Concr. Res. 9 (1979) 701–711.
[19] I. Maki, S. Chromy, Characterization of the alite phase in Portland cement clinker by microscopy, Il Cemento 3 (1978) 252–274.
[20] I. Maki, K. Goto, Factors influencing the phase constitution of alite in Portland cement clinker, Cem. Concr. Res. 12 (1982) 301–308.
[21] I. Maki, K. Kato, Phase identification of alite in Portland cement clinker, Cem. Concr. Res. 12 (1) (1982) 93–100.
[22] N. Yannaquis, M. Regourd, C. Mazières, A. Guinier, Polymorphism of the tricalcium silicate, Bull. Soc. Fr. Mineral. Cristallogr. 85 (3) (1962) 271–281.
[23] M. Regourd, Détermination des réseaux de cristaux microscopiques. Application aux différentes formes du silicate tricalcique, Bull. Soc. Fr. Mineral. Cristallogr. 87 (2) (1964) 241–272.
[24] N.I. Golovastikov, R.G. Matveeva, N.V. Belov, Crystal structure of the tricalcium silicate $3CaO \cdot SiO_2 = C_3S$, Sov. Phys. Crystallogr. 20 (4) (1975) 441.
[25] F. Nishi, Y. Takéuchi, The rhombohedral structure of tricalcium silicate at 1200 °C, Zeit Krist. 168 (1984) 197–212.
[26] A.M. Il'inets, Y.A. Malinovskii, Crystal structure of the rhombohedral modification of tricalcium silicate $Ca_3SiO_5$, Sov. Phys. Dokl. 30 (1985) 191.
[27] F. Ordway, Crystal structures of clinker constituents, Proc. of the 4th ISCC, Washington, 1960, pp. 39–58.
[28] T. Hahn (Ed.), International tables for crystallography, vol. 1, Kluwer Academic Publishers, Dordrecht, The Netherlands, 1952.
[29] K.E. Hudson, G.W. Groves, The structure of alite in Portland cement clinker TEM evidence, Cem. Concr. Res. 12 (1) (1982) 61–68.
[30] W. Sinclair, G.W. Groves, Transmission electron microscopy and X-ray diffraction of doped tricalcium silicate, J. Am. Ceram. Soc. 67 (1984) 325–330.
[31] W.G. Mumme, Crystal structure of tricalcium silicate from a Portland cement clinker and its application to quantitative XRD analysis, Neues Jahrb. Mineral. Mh. H 4 (1995) 145–160.
[32] J. Neubauer, H. Pöllmann, H.W. Meyer, Quantitative X-ray analysis of OPC clinker by Rietveld refinement, Proc. of the 10th ICCC, vol. 3, 1997, p. 3v007.
[33] M.-N. de Noirfontaine, M. Courtial, F. Dunstetter, G. Gasecki, M. Signes-Frehel, Tricalcium Silicate $Ca_3SiO_5$: the Major Compound of Anhydrous Portland Cement, 18th European Crystallographic Meeting ECM18, Glasgow, Scotland, 1999.
[34] M. Signes-Frehel, M. Bellotto, D. Ravaux, An Application of the Clinker Quantitative Analysis, 18th European Crystallographic Meeting ECM18, Glasgow, Scotland, 1999.
[35] M.-N. de Noirfontaine, Etude structurale et cristallographie du composé majoritaire du ciment anhydre: le silicate tricalcique, PhD thesis, Ecole Polytechnique (2000).
[36] M.-N. de Noirfontaine, M. Courtial, F. Dunstetter, G. Gasecki, M. Signes-Frehel, Tricalcium Silicate $Ca_3SiO_5$: the Major Compound of Anhydrous Portland Cement Revisited, 19th European Crystallographic Meeting (ECM 19), Nancy, France, 2000.
[37] M. Signes-Frehel, M.-N. de Noirfontaine, F. Dunstetter, Modelling of Alite: an Industrial Challenge, 19th European Crystallographic Meeting (ECM 19), Nancy, France, 2000.
[38] M.-N. de Noirfontaine, F. Dunstetter, M. Courtial, G. Gasecki, M. Signes-Frehel, Tricalcium silicate $Ca_3SiO_5$, the major component of anhydrous Portland cement: on the conservation of distances and directions and their relationship to the structural elements, Zeit Krist. 218 (2003) 8–11.
[39] M.-N. de Noirfontaine, F. Dunstetter, M. Courtial, Tricalcium silicate $Ca_3SiO_5$: from the superstructure analysis to the structure of the M1 Polymorph, Zeit Krist. (2003) (submitted).
[40] R. Berliner, C. Ball, P.B. West, Neutron powder diffraction investigation of model cement compounds, Cem. Concr. Res. 27 (4) (1997) 551–575.
[41] A.G. De La Torre, S. Bruque, J. Campo, M.A.G. Aranda, The superstructure of $C_3S$ from synchrotron and neutron powder diffraction an its role in quantitative phase analyses, Cem. Concr. Res. 32 (2002) 1347–1356.
[42] K. Urabe, T. Shirakami, M. Iwashima, Superstructure in a triclinic phase of tricalcium silicate, J. Am. Ceram. Soc. 83 (5) (2000) 1253–1258.
[43] K. Urabe, H. Nakanov, H. Morita, Structural modulations in monoclinic tricalcium silicate solid solutions doped with zinc oxide, M(I), M(II) and M(III), J. Am. Ceram. Soc. 85 (2002) 423.
[44] M. Courtial, M.-N. de Noirfontaine, F. Dunstetter, G. Gasecki, M. Signes-Frehel, Polymorphism of tricalcium silicate in Portland

cement: a fast visual identification of structure and superstructure, Powder Diffr. 18 (1) (2003) 7–15.
[45] M. Van Meerssche, J. Feneau-Dupont, Introduction à la Cristallographie et à la Chimie Structurale, Peeters, Leuven, 1984, p. 280.
[46] A.M. Il'inets, M.J. Bikbau, New rhombohedral modification $Ca_3SiO_5$ and mechanism of atomic transformation during the phase transition, in: XII European Crystallographic Meeting, Moscow, vol. 2, 1989, pp. 77–78.
[47] A.M. Il'inets, M.J. Bikbau, in: J. Haseln (Ed.), Phase Transitions in Dicalcium and Tricalcium Silicates, Diffraction Methods in Materials Science, Nova Science, 1992, pp. 161–175.
[48] M. Regourd, Les transformations polymorphiques du silicate tricalcique, Rev. Matér. Constr. 620 (1967) 167–176.
[49] M. Regourd, Cristallographie des constituants du clinker de ciment Portland, Bull. Liaison-Lab. Routiers No. Spécial 0 (1970) 58–73.
[50] M. Regourd, A. Guinier, Cristallochimie des constituants du clinker de ciment Portland, Proc. of the 6th ICCC, Moscow, 1974, pp. 201–215.
[51] M. Regourd, L'hydratation du ciment Portland, Le béton hydraulique, Presses LCPC, Paris, 1982, pp. 193–221 (Chap. 11).
[52] M. Regourd, A.I. Boikova, Polymorphism and structure of Portland phases, Proc. of the 9th ICCC, New-Delhi, Part II: Chemistry, Structure Properties and Quality of Clinker, vol. 1, The National Council for Cement Building Materials, New Delhi, 1992, p. 3.
[53] G. Yamaguchi, H. Miyabe, Precise determination of the 3CaO. $SiO_2$ cells and interpretation of their X-ray diffraction patterns, J. Am. Ceram. Soc. 43–4 (1960) 219–224.
[54] I. Maki, Relationship of processing parameters to clinker properties; influence of minor components, Proc. of the 8th ICCC, Rio de Janeiro, vol. 1, 1986, pp. 34–47, Abla Grafica e Editoria Ltda, Rio de Janeiro.
[55] H.F.W. Taylor, The Chemistry of Cements, Academic Press, London, 1964.